Computational Analysis and Optimization of Wire – Sandwiched Micro Heat Pipes

Rag, R. L.[1] and Sobhan, C. B.[2]
Nanotechnology Research Laboratory, National Institute Technology Calicut, India 673 601

Abstract
Micro heat pipes are a promising option for the thermal management of microelectronic systems with high heat flux dissipation rates. A computational analysis is performed on wire-sandwiched micro heat pipes, a relatively new design of micro heat pipes, which utilizes an array of wires sandwiched between metallic plates to produce the flow channels. A transient one-dimensional model incorporating the longitudinal variations in the flow cross sections of the liquid and vapor media has been utilized, while developing the governing equations for the analysis. A fully implicit finite difference scheme is utilized to obtain solutions for the velocity, pressure and temperature distributions in the vapor and the liquid phases. The performance of the heat pipe has been obtained, with the effective thermal conductivity as the indicator, and extensive optimization studies have been performed with respect to the geometric parameters namely the length of the heat pipe sections, the diameter and pitch of the wires in the sandwiched structure, and operational parameters namely the heat input and the condenser heat transfer coefficient. The effects are correlated using a regression analysis, and further utilized in obtaining the optimal design of the micro heat pipe within a range of parameters. The analysis provides guidelines for the geometric design of wire-sandwiched micro heat pipes for heat dissipation from micro electronic chips, based on the results corresponding to the thermal management conditions encountered in such applications.

NOMENCLATURE

A	=	area of cross section, m^2
C	=	specific heat, J/kg K
D_H	=	hydraulic diameter of the channel, m
E	=	total energy per unit volume, J/m^3
f	=	friction factor
h_{fg}	=	latent heat of vaporization, J/kg
h_o	=	heat transfer coefficient, W/m^2K
k	=	thermal conductivity, W/m K
k*	=	thermal conductivity normalized with respect to copper
L	=	length of the heat pipe, m
P	=	perimeter, m
p	=	pressure, Pa
P_w	=	pitch of the wires (center to center distance of the wire), m
Q	=	heat, W
q	=	heat flow rate, W/m^2
R	=	universal gas constant, J/kg K
r_m	=	radius of the meniscus, m
Re	=	Reynolds number

[1]Ph. D. Scholar, Department of Mechanical Engineering
[2]Professor, School of Nano Science and Technology. Corresponding author. E Mail: csobhan@nitc.ac.in

R_w = radius of the wire, m
R_{min} = minimum meniscus radius, m
t = time, s
T = temperature, K
ΔT = temperature difference, $T-T_{amb,}$ K
u = axial velocity, m/s
v = velocity, m/s
x = axial coordinate
α = contact angle, deg.
μ = dynamic viscosity, kg/m s
ρ = density, kg/m^3
σ = surface tension, N/m

Subscripts
amb = ambient
ave = average
a = adiabatic section
c = condenser section
e = evaporator section
eff = effective
h = hydraulic
i = interface
l = liquid
li = liquid-interface
lw = liquid-wall
max = maximum
min = minimum
sat = saturation
v = vapor
vi = vapor interface
vw = vapor-wall

1. INTRODUCTION

The micro heat pipe is a heat transfer device of high effective conductance, which utilizes phase change of the working fluid and the capillary action at the corners of flow passages for its operation, as described extensively in the literature [1-5]. Though the micro heat pipe also utilizes similar thermal phenomena as a conventional heat pipe [6], and consists of the evaporator, adiabatic and condenser sections, the absence of a wick structure and the smaller size make the micro heat pipe physically different from the conventional heat pipe. The sharp corners of the non-circular cross sections of the micro heat pipes provide the liquid arteries for the transport of the liquid from its condenser section to the evaporator section [2, 3]. Schematic of a typical micro heat pipe channel of the design analyzed in the present paper is given in Figure 2, which gives the configuration of the sections of the device.

The first attempt to utilize an array of micro heat pipes for thermal management of electronic devices was made by Cotter [2] who proposed the fabrication of such devices as an integral part of micro electronic devices. In a typical design of micro heat pipes, heat addition at the evaporator section generates vapor from the liquid phase of the working fluid, which is at its saturation condition, and makes the vapor flow from the evaporator section to the condenser section. If sufficient capillary pressure difference is provided by the corners of the passages, the liquid is transported back to the evaporator section from the externally cooled condenser section, thus setting up a fluid circuit in the device. The small cross-sectional dimensions of the channels required for this phenomenon to take place also gives an opportunity to construct the micro heat pipe as a miniature heat sink or heat spreader. As the heat carrying capacity of each such channel is limited, arrays of micro heat pipes are used in a compact heat sink or heat spreader, for various heat transfer applications [5]. Theoretical and experimental investigations on micro heat pipes with trapezoidal, triangular and rectangular cross sections can be found in the literature, as will be reviewed here. The wire – sandwiched micro heat pipes, which is analyzed in this paper, is a novel design of micro heat pipes [3, 7], constructed by sandwiching an array of wires in between two plates to provide flow passages.

Based on the first steady state model of the micro heat pipe by Cotter [2], Babin et al. [4] developed a model for trapezoidal micro heat pipes (micro heat pipes with a trapezoidal cross section) to predict the maximum heat transport capacity, using conventional modeling methods outlined by Chi [5]. Khrustalev and Faghri [8] presented a detailed mathematical model for the heat and mass transfer processes in micro heat pipes with a rectangular cross section, and compared the results with experimental data presented by Wu and Peterson [9] and Wu et al. [10]. A one dimensional steady state model for the evaporator and the adiabatic sections of a triangular micro heat pipe was developed by Longtin et al. [11] assuming uniform vapor temperature throughout its length, and incorporating the interfacial shear stress and body force terms in the momentum equation.

A steady state mathematical model for the maximum heat transport capability of a micro heat pipe was developed by Peterson and Ma [12], which considered the governing equations for fluid flow and heat transfer in the evaporating thin film region. The maximum heat transfer capacity of copper-water micro heat pipes was explored by Hopkins et al. [13] using a one dimensional model for predicting the capillary limitation. In this analysis, the liquid-vapor meniscus was divided into two regions depending on whether the contact angle is constant at the evaporator or varying along the adiabatic and condenser sections.

An experimental investigation of the transient behavior of the micro heat pipe was performed by Wu and Peterson [9], which indicated a major liquid flow reversal due to an imbalance of pressure, during the transient period. A mathematical model was developed by Ma et al. [14] for liquid friction factor in irregular grooves, relevant to the micro heat pipe geometry. This model considered interfacial shear stress due to the liquid-vapor frictional interaction. A transient model for a triangular micro heat pipe consisting of an evaporator section and a condenser section was developed by Sobhan et al. [15]. In this model, the differential forms of the momentum and energy equations were solved, along with the interfacial mass conservation equations across the meniscus, and the Laplace-Young equation containing the meniscus radius. Sobhan and Peterson [16] further explored this model solving the governing equations to analyze the performance of the heat pipe for a much wider range of parametric variations. A comprehensive review of the analysis of micro heat pipes found in the literature, and a quantitative comparison of the performance of various designs are presented in a recent publication by Sobhan et al. [17].

The wire-sandwiched (wire-bonded) micro heat pipe [3] is one of the latest innovations in micro heat pipes, proposed for use in conventional electronic cooling applications and also in advanced applications such as in spacecrafts. This device can be fabricated by sintering an array of wires between two thin metal plates. The sharp corners formed between the plate and the wires serve as liquid arteries [3, 7]. A few publications dealing with the theoretical analysis of the flow and heat transfer process in wire-sandwiched micro heat pipes can be found in the literature [7, 18]. The wire-bonded micro heat pipe was conceptualized, modeled and analyzed by Wang and Peterson [7] to obtain the effects of various parameters on its maximum heat transport capacity. Launay et al. [18] investigated the effects of contact angle, fluid type, corner angle and fill charge on the performance of a wire-plate micro heat pipe array. However, these investigations have not incorporated the fluid cross-sectional area variation along the heat pipe as a function of the position, in a differential formulation.

In the present study, a computational analysis is performed on the wire-sandwhiched micro heat pipe, with an objective to understand and quantify the influence of various geometrical and operational parameters on its performance. The field variables in the flow of the working fluid are computed from the governing equations, and the temperature distribution is used for calculating the effective thermal conductivity which is the performance indicator of the heat pipe. A multiple linear regression analysis to correlate the performance, followed by an optimization study on the correlation, are performed to obtain the optimum combination within a prescribed range of parameters, which gives the best value of the effective thermal conductivity.

2. FORMULATION

The wire-sandwiched micro heat pipe essentially consists of an array of channels, formed by sandwiching an array of wires between two metal plates. Each channel in the array acts as an individual micro heat pipe as shown in Figure 1. An externally heated evaporator, an adiabatic section with no external heat transfer and a condenser section subjected to convective cooling are the distinct sections of the micro heat pipe. The cross sectional areas of the liquid and the vapor change longitudinally from the evaporator end to the condenser end, as represented in Fig 1(c). Since the variations of the field variables are much more significant in the longitudinal direction than in the other directions, a one dimensional model can be used for the analysis.

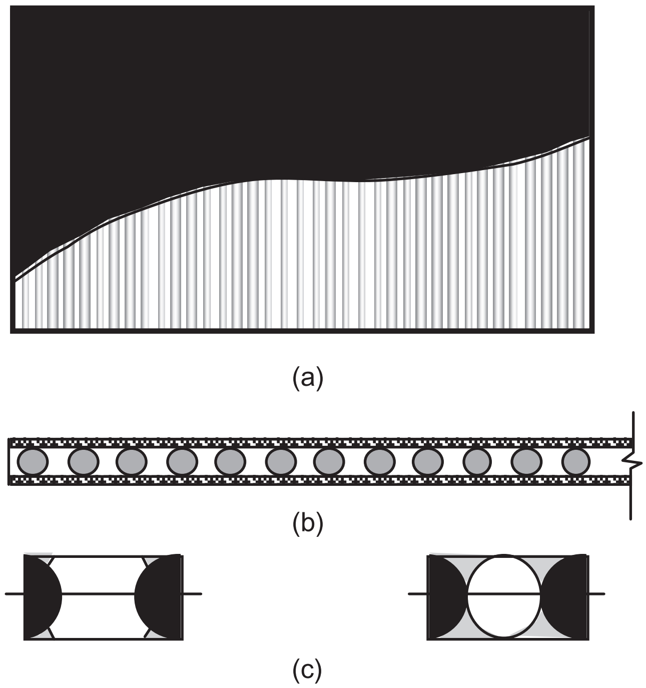

Figure 1. Schematic of the wire-sandwiched micro heat pipe construction [3, 7]

The mathematical model is based on the following assumptions:

1. Laminar flow prevails in both the liquid and the vapor phases.
2. No slip boundary condition exists at the solid-fluid boundaries, as has been verified through a Knudsen number calculation for the physical dimensions and the working fluid.
3. The vapor is at its saturation pressure, corresponding to the working temperature.
4. The thermophysical properties of the vapor and liquid phases are constant along the heat pipe, as the temperature variation is small.

The local meniscus radius of the vapor – liquid interface can be computed using the Laplace – Young equation, which connects it to the fluid pressures through the surface tension. The major governing equations are the differential equations for mass, momentum and energy conservation. The pressure and the temperature of the vapor are be linked through the equation of state. As a first approximation, in the liquid phase, the Hagan – Poisselleuie equation is used for calculating the pressure, which is corrected iteratively by re-substituting in the momentum equation. The methodology of the mathematical formulation has been presented earlier while analyzing triangular micro heat pipes [3], whereas the geometry of the passages is different in the present case. The area variations in the longitudinal direction, with the appropriate geometry for the wire-sandwiched heat pipe passages, are incorporated in the differential equations. The geometrical derivations pertaining to the calculation of the cross sectional areas of the fluid streams as a function of the local meniscus radius are also given below, along with the mathematical formulation.

Laplace-Young Equation:

$$p_v - p_l = \frac{\sigma}{r} \tag{1}$$

Vapor continuity equation:
In the evaporator section

$$A_v \frac{du_v}{dx} + u_v \frac{dA_v}{dx} + P_i v_{iv} = 0 \tag{2}$$

In the adiabatic section

$$A_v \frac{du_v}{dx} + u_v \frac{dA_v}{dx} = 0 \tag{3}$$

In the condenser section

$$A_v \frac{du_v}{dx} + u_v \frac{dA_v}{dx} - P_i v_{iv} = 0 \tag{4}$$

Vapor momentum equation:

$$\rho_v \left[u_v^2 \frac{\partial A_v}{\partial x} + 2 A_v u_v \frac{\partial u_v}{\partial x} \right] + A_v \frac{\partial p_v}{\partial x} + \rho_v A_v g \sin\theta - \frac{1}{2} P_{vw} \rho_v u_v^2 f_{vw} - \frac{1}{2} P_i \rho_v u_v^2 f_{iv} = \rho_v A_v \frac{\partial u_v}{\partial t} \tag{5}$$

Vapor energy equation:
In the evaporator section

$$A_v \frac{\partial E_v}{\partial t} + \frac{\partial}{\partial x}\left[u_v A_v \left(E_v + p_v \right) \right] = \frac{\partial}{\partial x}\left\{ \frac{4}{3} \mu_v u_v A_v \frac{\partial u_v}{\partial x} + K_v A_v \frac{\partial T_v}{\partial x} \right\} + q P_{vw} + h_{fg} v_{iv} \rho_v P_i + \frac{1}{2} \rho_v u_v^2 f_{iv} u_v p_{iv} + \frac{1}{2} \rho_v u_v^2 f_{vw} u_v P_{vw} \tag{6}$$

$$\text{Where } E_v = \rho_v \left(c_v T + \frac{1}{2} u_v^2 \right)$$

In the adiabatic section

$$A_v \frac{\partial E_v}{\partial x} + \frac{\partial}{\partial x}\left[u_v A_v \left(E_v + P_v \right) \right] = \frac{\partial}{\partial x}\left\{ \frac{4}{3} \mu_v u_v A_v \frac{\partial u_v}{\partial x} + K_v A_v \frac{\partial T_v}{\partial x} \right\} + \frac{1}{2} \rho_v u_v^2 f_{iv} u_v p_{iv} + \frac{1}{2} \rho_v u_v^2 f_{vw} u_v P_{vw} \tag{7}$$

In the condenser section

$$A_v \frac{\partial E_v}{\partial t} + \frac{\partial}{\partial x}\left[u_v A_v \left(E_v + p_v\right)\right] = \frac{\partial}{\partial x}\left\{\frac{4}{3}\mu_v u_v A_v \frac{\partial u_v}{\partial x} + K_v A_v \frac{\partial T_v}{\partial x}\right\} + h_0 P_{vw}\Delta T - h_{fg} v_{iv}\rho_v P_i + \frac{1}{2}\rho_v u_v^2 f_{iv} u_v P_{iv} + \frac{1}{2}\rho_v u_v^2 f_{vw} u_v P_{vw} \tag{8}$$

Liquid continuity equation:
In the evaporator section

$$A_l \frac{du_l}{dx} + u_l \frac{dA_l}{dx} - P_i v_{il} = 0 \tag{9}$$

In the adiabatic section

$$A_l \frac{du_l}{dx} + u_l \frac{dA_l}{dx} = 0 \tag{10}$$

In the condenser section

$$A_l \frac{du_l}{dx} + u_l \frac{dA_l}{dx} + P_i v_{il} = 0 \tag{11}$$

Liquid momentum equation:

$$-\rho_l \left[u_l^2 \frac{\partial A_l}{\partial x} + 2A_l u_l \frac{\partial u_l}{\partial x}\right] - A_l \frac{\partial p_l}{\partial x} + \rho_l A_l g \sin\theta - \frac{1}{2}P_{lw}\rho_l u_l^2 f_{lw} - \frac{1}{2}P_i \rho_l u_l^2 f_{il} = \rho_l A_l \frac{\partial u_l}{\partial t} \tag{12}$$

Liquid energy equation:
In the evaporator section

$$A_l \frac{\partial E_l}{\partial t} + \frac{\partial}{\partial x}\left[u_l A_l \left(E_l + p_l\right)\right] = \frac{\partial}{\partial x}\left\{\frac{4}{3}\mu u_l A_l \frac{\partial u_l}{\partial x} + K_l A_l \frac{\partial T_l}{\partial x}\right\} + qP_{lw} - h_{fg} v_{il}\rho_l P_i + \frac{1}{2}\rho_l u_l^2 f_{il} u_l P_i + \frac{1}{2}\rho_l u_l^2 f_{lw} u_l P_{lw} \tag{13}$$

In the adiabatic section

$$A_l \frac{\partial E_l}{\partial x}\left[u_l A_l \left(E_l + p_l\right)\right] = \frac{\partial}{\partial x}\left\{\frac{4}{3}\mu_l u_l A_l \frac{\partial u_l}{\partial x} + K_l A_l \frac{\partial T_l}{\partial x}\right\} + \frac{1}{2}\rho_l u_l^2 f_{il} u_l p_{iv} + \frac{1}{2}\rho_l u_l^2 f_{il} u_l P_{lw} \tag{14}$$

In the condenser section

$$A_l \frac{\partial E_l}{\partial t} + \frac{\partial}{\partial x}\left[u_l A_l \left(E_l + p_l\right)\right] = \frac{\partial}{\partial x}\left\{\frac{4}{3}\mu u_l A_l \frac{\partial u_l}{\partial x} + K_l A_l \frac{\partial T_l}{\partial x}\right\} - h_0 P_{lw}\Delta T + h_{fg} v_{il}\rho_l P_i + \frac{1}{2}\rho_l u_l^2 f_{il} u_l P_i + \frac{1}{2}\rho_l u_l^2 f_{lw} u_l P_{lw} \tag{15}$$

Equation of state for the vapor:

$$p_v = \rho_v R_v T_v \tag{16}$$

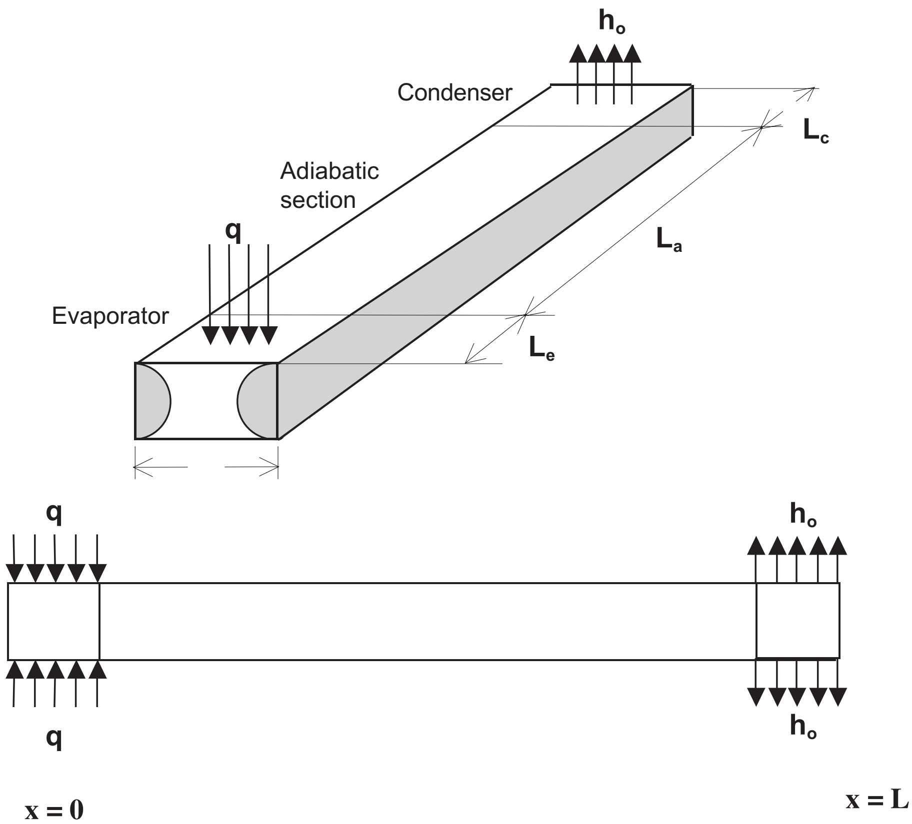

Figure 2. Configuration of a single micro heat pipe in the array

Hagen-Poiseuille equation as first approximation for the liquid flow:

$$\frac{\partial p_l}{\partial x} = -\frac{8\mu_l u_l}{\frac{D_H^2}{4}} \tag{17}$$

Boundary conditions

At x=0 and x=L

$$u_l = 0;\ u_v = 0;\ \frac{\partial T}{\partial x} = 0$$

At x=0

$$p_v - p_l = \frac{\sigma}{r_{\min}}$$

The minimum meniscus radius is obtained from literature as 32 x 10^{-5} m [7].

Initial conditions:

At t=0, for all x

$$p_v = p_l = p_{sat} \ ; \ T_v = T_l = T_{sat}$$

The friction factors appearing in the governing equations can be generally expressed as

$$f = \frac{k}{\text{Re}} \tag{18}$$

where “k” is a constant that depends on the geometry of the heat pipe channel.

The value of ‘k’ for the vapor and the liquid depends on the flow cross sections of both the vapor and the liquid. The cross section of the vapor passage varies continuously from the evaporator to the condenser section. It can be assumed that the vapor core is having approximately rectangular cross section at the evaporator and the circular cross section at the condenser as shown in Figure 1(c). The liquid at every corner is assumed to have an almost triangular cross section. The appropriate values of ‘k’ corresponding to the geometries mentioned above are obtained from the literature [19].

The interfacial meniscus radius is the variable which determines the local cross sectional areas of both the liquid and the vapor, which progressively along the length. The interfacial meniscus is shown schematically in Figure 3. Based on the geometry, the relevant geometric quantities can be obtained as follows:

Area of liquid $A_l = 8R_w r_m Sin\beta_1 Sin\beta_2 - 4R_w^2\left(\beta_1 - Sin\beta_1 Cos\beta_1\right) - 4r_m^2\left(\beta_2 - Sin\beta_2 Cos\beta_2\right)$ (19)

Area of vapor $A_v = R_w\left(2w - \pi R_w\right) - A_l$ (20)

Liquid – vapor interface perimeter $p_{iv} = p_{il} = 8r_m\beta_2$ (21)

Liquid-wall contact area $p_l = 2R_w\left(\beta_1 + \tan\beta_1\right)$ (22)

Vapor-wall contact area $p_v = 2(w + \pi R_w) + 8(r_m\beta_2 - R_w \tan\beta_1 - R_w\beta_1)$ (23)

Relation between α, β_1 and β_2: $\beta_1 + \beta_2 + \alpha = \frac{\pi}{2}$ (24)

$$R_w Sin^2\beta_1 = r_m Cos\beta_1 Sin\beta_2 \tag{25}$$

$$\beta_1 = \tan^{-1}\left(\left(\frac{1}{2R_w}\right)\left\{-r_m Sin\alpha + \left[\left(r_m Sin\alpha\right)^2 + 4R_w r_m Cos\alpha\right]^{\frac{1}{2}}\right\}\right) \tag{26}$$

The constructional details of the micro heat pipe considered in the analysis, and the properties of the working fluid are given in Table 1.

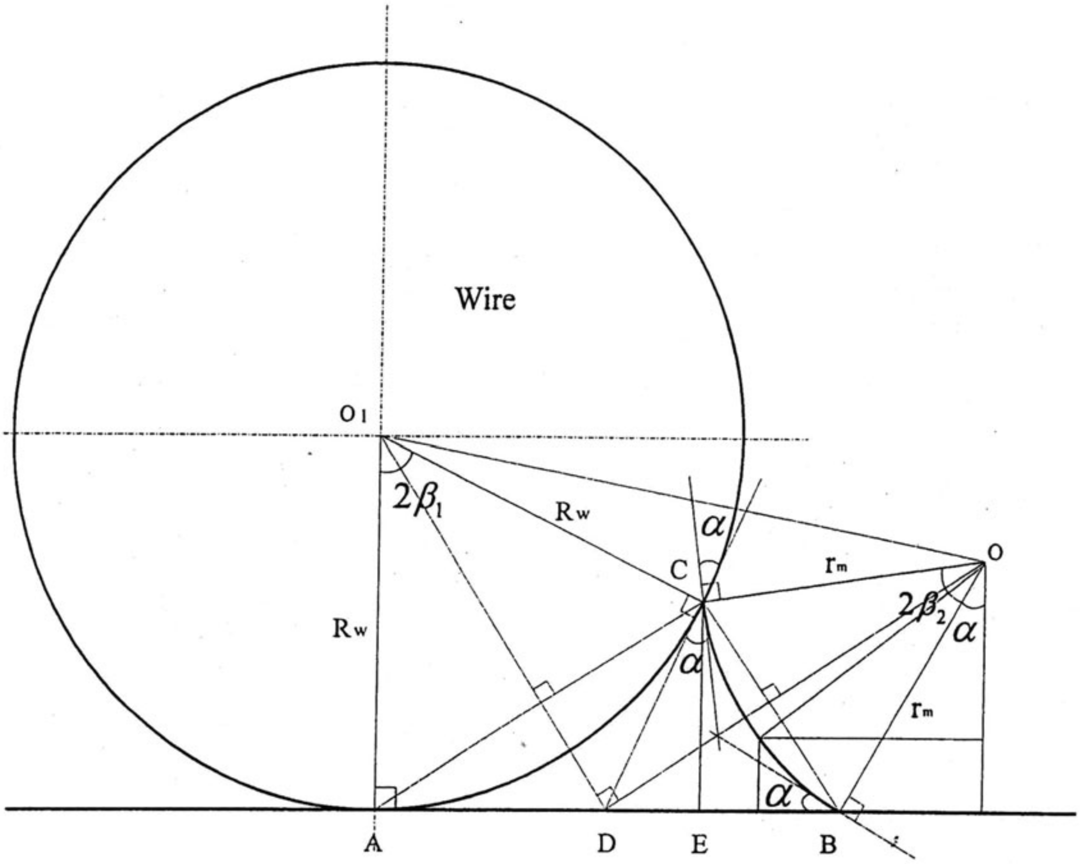

Figure 3. Geometry of the interface meniscus in the wire-sandwiched micro heat pipe [5]

Table 1. Details of the Physical Problem

Solid material	Copper
Working fluid	Water
Length of the heat pipe	125 mm (base-line case),120mm,121mm 122mm, 123mm, 124 mm,127.5mm, 128mm, 130mm
Radius of wire	0.8 mm (base-line case), 0.825mm, 0.85mm, 0.875mm, 0.9mm
Pitch of the wires	2.0 mm (base-line case), 2.1mm, 2.2mm, 2.3 mm, 2.4mm
Length of the evaporator	20 mm
Length of the adiabatic section	85mm (base-line case), 82mm, 88mm
Length of the condenser	20 mm (base-line case), 15mm, 16mm, 17mm, 18mm, 19mm, 20mm, 22.5mm, 25mm
Density of vapor	0.0256 kg/m^3
Density of liquid	998.2 kg/m^3
Thermal conductivity of liquid	0.613 W/m K
Thermal conductivity of vapor	19.6×10^{-3} W/m K
Viscosity of liquid	1.003×10^{-3} N s/m^2
Viscosity of vapor	9.09×10^{-6} N s/m^2
Surface tension	0.0718 N/m

3. NUMERICAL SOLUTION

A fully implicit finite difference scheme based on central differences is used for solving the coupled governing equations. The solution procedure has been discussed in the literature [15]. The steps involved in the procedure are summarized below:

1. Obtain the local meniscus radius using the Laplace – Young equation.
2. Using the vapor momentum equation obtain the vapor velocity.
3. Obtain the interfacial vapor velocity using the vapor continuity equation and calculate the interfacial liquid velocity applying the interface mass balance.
4. Obtain the vapor temperature from the vapor energy equation.
5. Calculate the vapor pressure using the equation of state for the vapor.
6. From the liquid continuity equation, obtain the liquid velocity derivatives in terms of the interfacial liquid velocity and substitute them in the liquid momentum equation. Solve the liquid momentum equation to obtain the liquid velocity.
7. Calculate the liquid pressure using Hagen- Poiseuille equation. Substitute the liquid pressure again in the liquid momentum equation and iterate for spatial convergence.
8. Obtain the liquid temperature from the liquid energy equation.

An unsteady state formulation is used, and the steady state results are obtained using an implicit time stepping algorithm, applied through a finite difference scheme with successive under-relaxation to suppress divergence. Through grid refinement and use of small time-step sizes, stable and converged results are obtained. The overall energy balance between the evaporator and condenser sections at steady state, as shown in Figure 4, is also used as a means of checking the accuracy of the computation, apart from the constant values of the field variables indicating steady state.

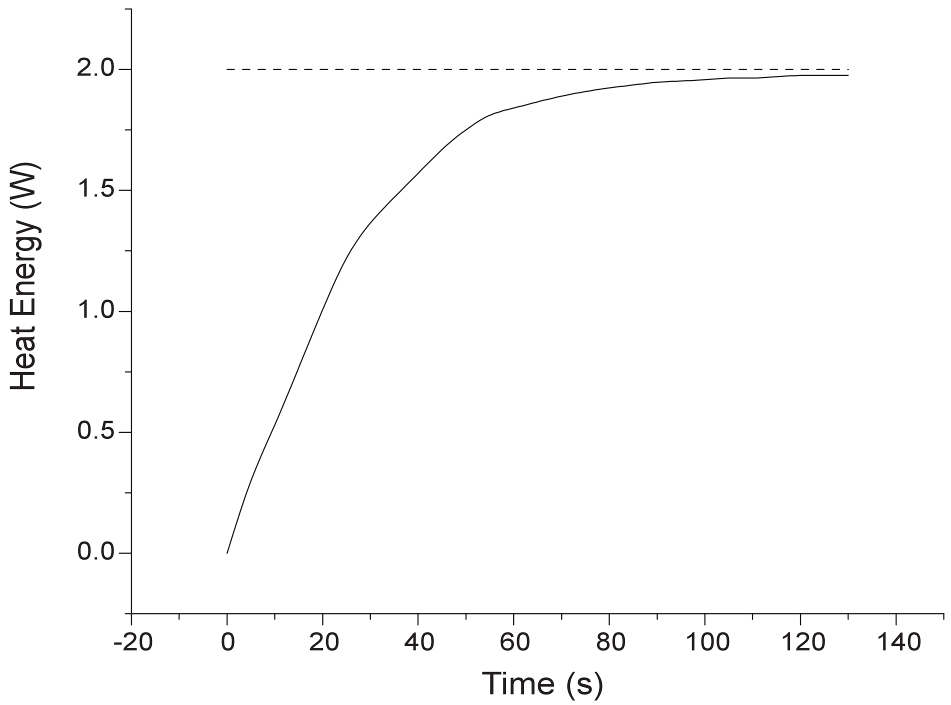

Figure 4. Transient variation of heat transfer at the condenser section for an input heat flux of 2.5W/cm^2 and a condenser heat transfer coefficient of 550 W/m^{2}K. The calculated heat input at the evaporator section corresponding to the base-line case is 2 W. The energy balance at the steady state is obvious.

4. RESULTS AND DISCUSSIONS

For benchmarking the computational approach, the calculated values were compared with the maximum evaporator temperature (Te_{max}), the average Temperature of the adiabatic section (Ta_{ave}) and the minimum condenser temperature (Tc_{min}) on the surface, as reported in the literature for the case of a wire sandwiched micro heat pipe [7]. The reported values for the input heat flux (0.5167 W/cm^2), wire diameter (0.813 mm) and condenser end temperature (313K) were utilized in the computation. Though the material fluid combination (acetone – aluminum system) used in [7] was different, the results were found to compare well in their trends, as depicted in Figure 5.

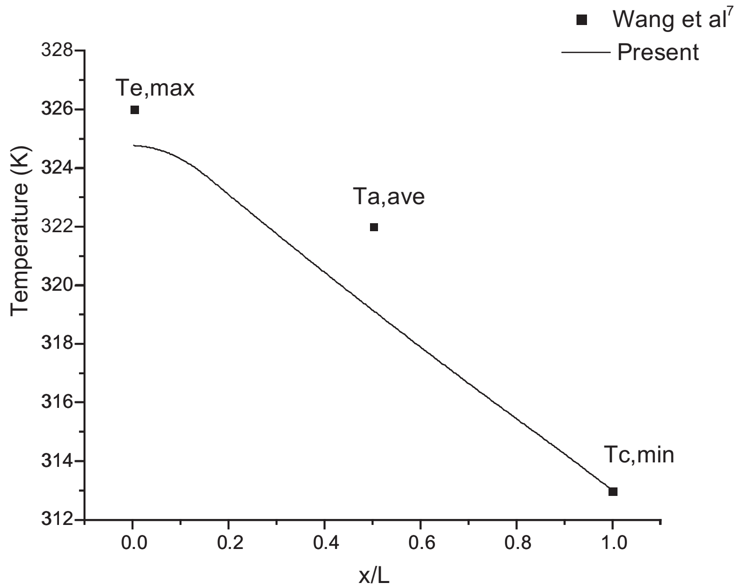

Figure 5. Comparison of the steady state temperature profile for an input heat flux of 0.52 W/cm^2 and a condenser end temperature of 313 K, with corresponding experimental results for an acetone-aluminum system [7].

Distribution of the field variables at the steady state

The distributions of the interfacial meniscus, velocity, temperature and pressure at the steady state for an input heat flux of 2.5 W/cm^2 and condenser heat transfer coefficient of 550 W/m^{2}K are shown in Figure 6 to Figure 10. The meniscus radius is calculated using the Laplace – Young equation which relates the vapor and the liquid pressures and the meniscus radius at any axial position. Since the pressure difference between the vapor and the liquid decrease progressively from the evaporator end to the condenser end, the meniscus radius increases along the length correspondingly. The nature of variation agrees with the meniscus radius distributions for a triangular micro heat pipe, as presented the literature [15], with the minimum value at the evaporator and the maximum at the condenser end.

The normalized steady state vapor and liquid velocity distributions are shown in Figure 7 and Fig 8, respectively. The magnitude of the vapor velocity is higher than the liquid velocity due to the appreciable difference in the densities of the vapor and the liquid. The negative values of the liquid velocity indicate the direction of flow of the liquid from the condenser to the evaporator end. The vapor velocity increases along the evaporator section and decreases along the condenser side due to the progressive mass addition and depletion in these sections. The variation of the liquid velocity is found to be non-linear in the condenser section due to the significant longitudinal variation in the cross sectional area of the liquid stream. In the adiabatic section, the velocity gradients are lower compared to those in the other two sections due to the absence of any significant heat addition and phase change.

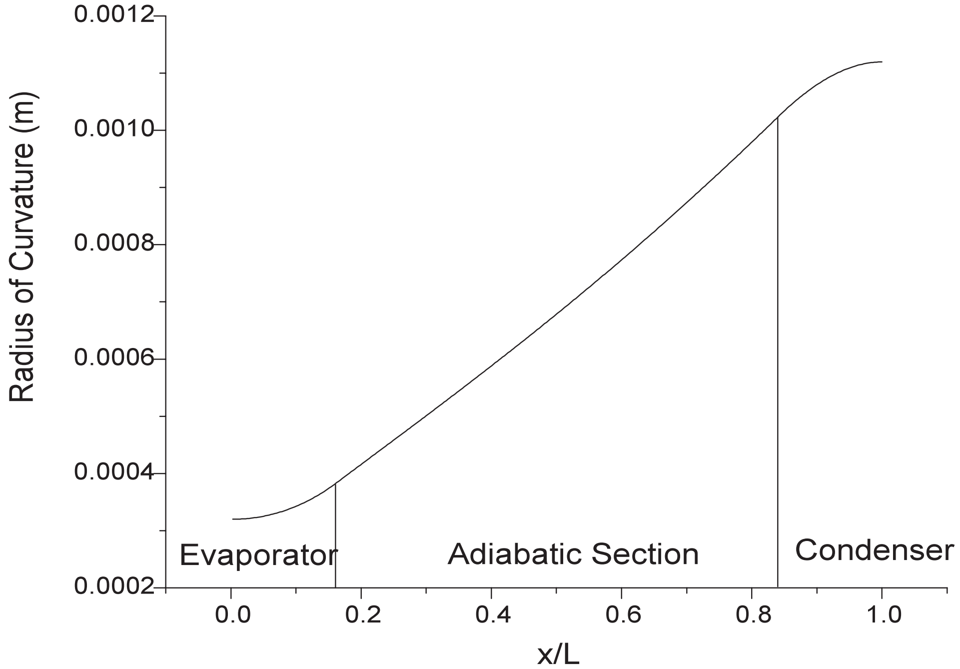

Figure 6. Distribution of the radius of curvature of the liquid-vapor interface meniscus along the micro heat pipe. The graph corresponds to an input heat flux of 2.5 W/cm^2 and a condenser heat transfer coefficient of 550 W/m^{2}K.

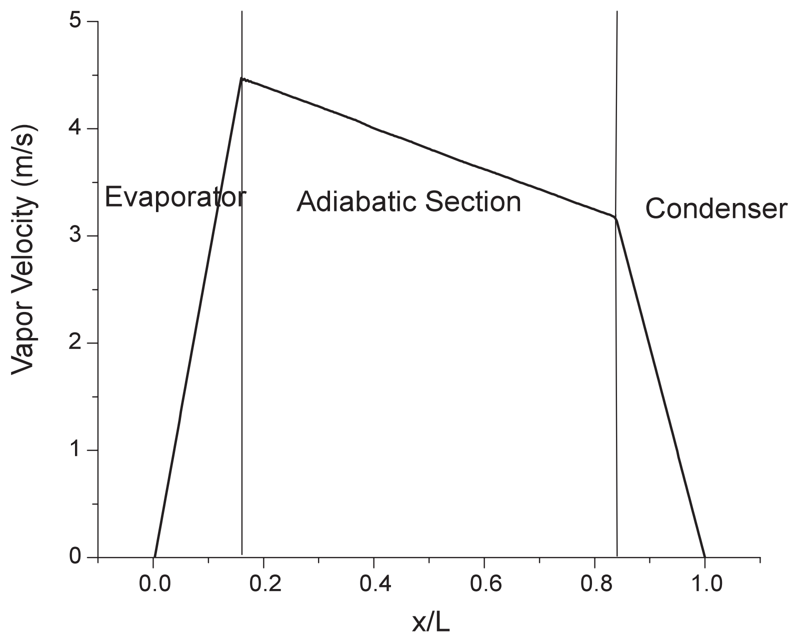

Figure 7. Vapor velocity distribution for a heat input of 2.5 W/cm^2 and condenser heat transfer coefficient of 550 W/m^2 K

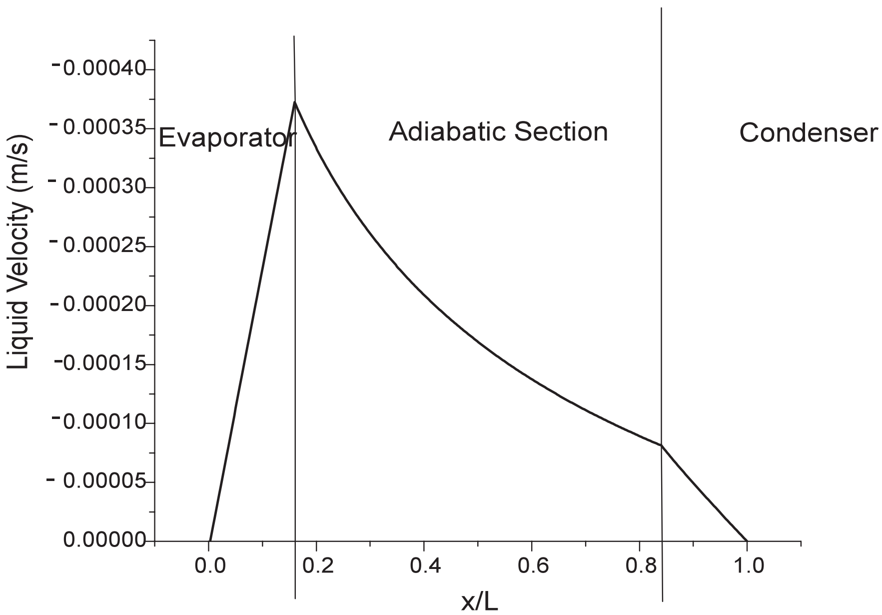

Figure 8. Liquid velocity distribution for a heat input of 2.5 W/cm^2 and condenser heat transfer coefficient of 550 W/m^2 K

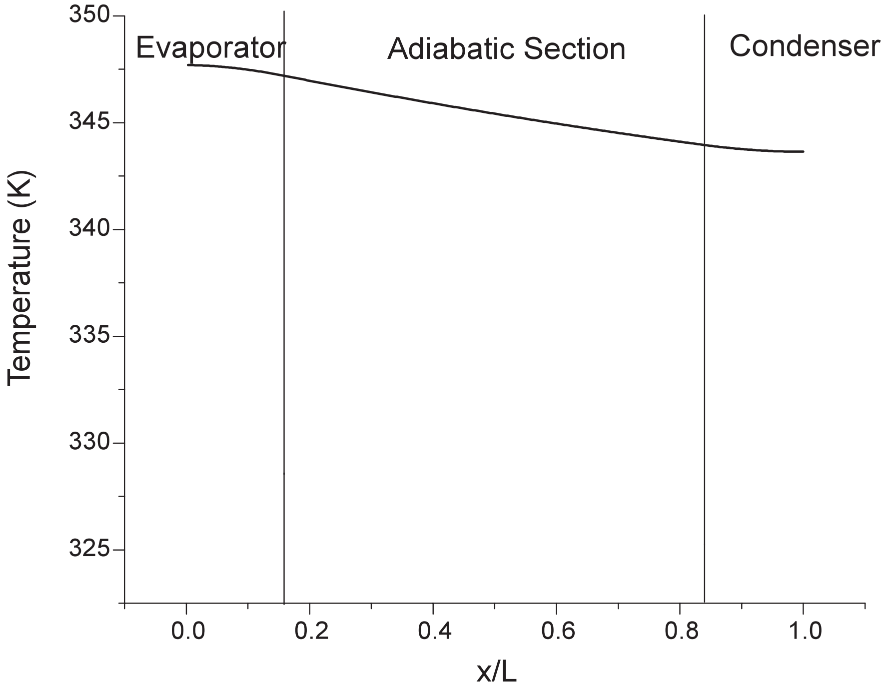

Figure 9. Steady state temperature distribution for a heat input of 2.5 W/cm^2 and a condenser heat transfer coefficient of 550 W/m^2 K

The longitudinal distribution of the steady state vapor temperature is shown in Figure 9. It is found that the effect of the evaporator and condenser sections propagate to the adiabatic section also to some extent, as indicated by smoothness of the curves at the junctions between the sections. Similar results of the propagation of the heating and cooling effects into the adiabatic section due to axial conduction effects have been discussed earlier in literature for conventional heat pipes [20]. The pressure distributions in the vapor and the liquid phases are shown in Figure 10. The pressure drop in the liquid is larger than that in the vapor, due to the large density of the liquid compared to the vapor. The results are typical for micro heat pipes, and agree with those obtained for triangular micro heat pipes [15, 16].

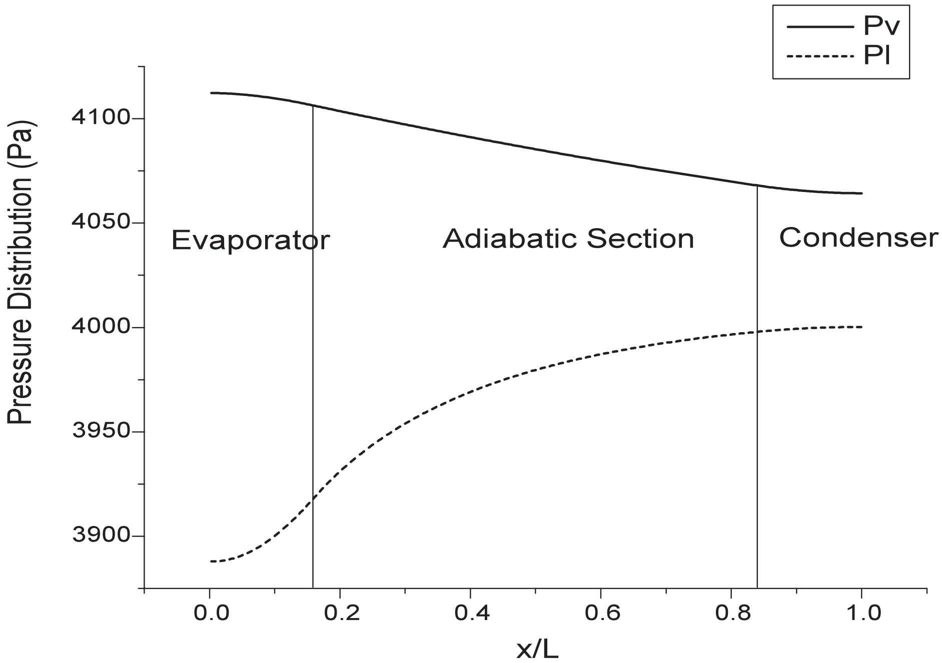

Figure 10. Longitudinal pressure distribution in the wire-sandwiched micro heat pipe. The heat input is 2.5 W/cm^2 and the condenser heat transfer coefficient is 550 W/m^2 K.

5. PERFORMANCE EVALUATION

The effective thermal conductivity is a performance indicator that helps to compare various designs of the micro heat pipes [15, 16]. The effective thermal conductivity is defined on the basis of the Fourier's law of heat conduction as follows:

$$k_{eff} = \frac{Q}{A_c \frac{\Delta T}{L}} \tag{27}$$

The above equation essentially compares the heat transfer in the micro heat pipe, with that in a solid conductor, to obtain an effective value of thermal conductivity. A large value of the effective thermal conductivity indicates that the heat pipe operates close to isothermal, for a given heat transport [3, 5].

Effects of operational and geometric parameters on the performance

The temperature distributions obtained from the computation are utilized to calculate the effective thermal conductivity values. Fig 11 shows the variation of the effective thermal conductivity, normalized with respect to the thermal conductivity of copper (termed effective thermal conductivity ratio) for cases with the input heat flux varying from 2.4 W/cm^2 to 2.5 W/cm^2. From a comparison of the temperature distributions as shown in Fig 12, it is clear that as the input heat flux is increased, the temperature drop between the longitudinal ends of the micro heat pipes gets reduced, thus resulting in an increased effective thermal conductivity. This is understood to be due to the increased vapor velocities at higher heating levels, which in turn effectively transmit the heat from the evaporator to the condenser section. The effective thermal conductivity decreases due to an increase in the condenser

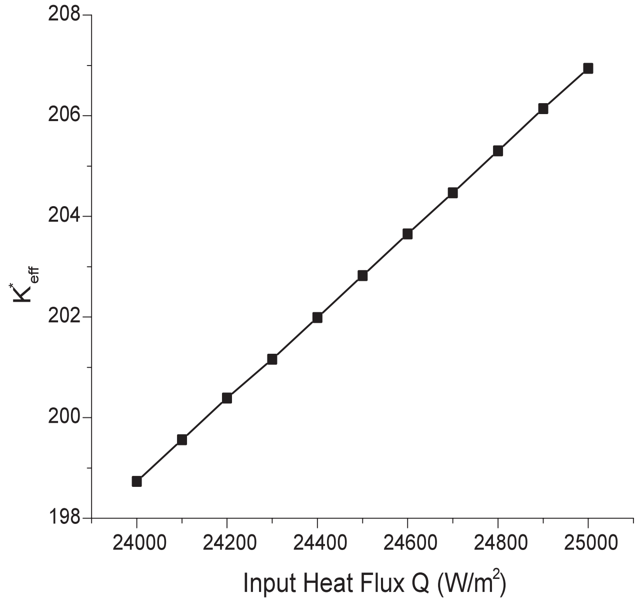

Figure 11. Variation of Effective Thermal Conductivity with heat input

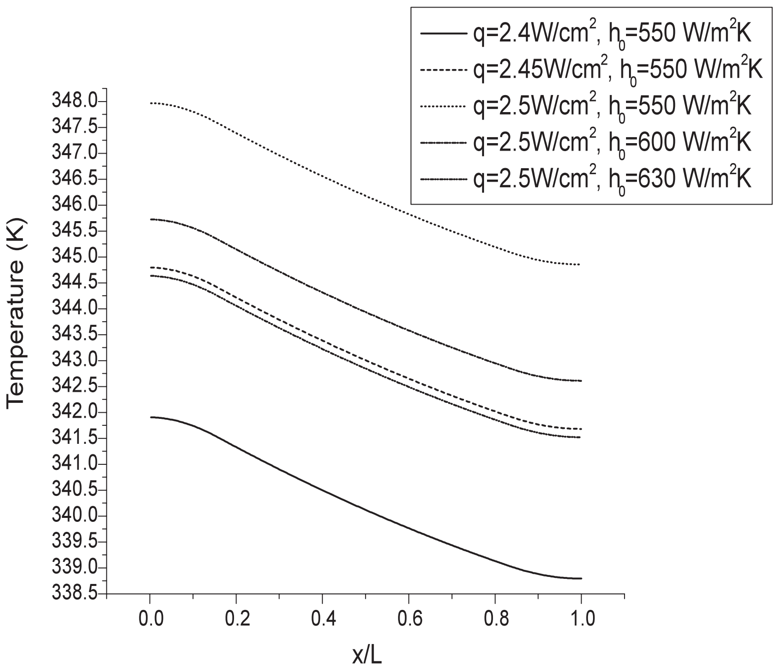

Figure 12. Steady state temperature distributions for various operational parameters (Input heat flux varies from 2.4 to 2.5 W/cm^2 and the condenser heat transfer coefficient varies from 550 to 630 W/m^{2}K)

heat transfer coefficient as shown Figure 13. This effect is due to the increased temperature drop between the ends of the micro heat pipes under such conditions. Though the heat transfer capability is not affected by this, the micro heat pipe deviates from its isothermal nature when the condenser heat transfer coefficient is excessively increased. The effects of both the input heat flux and the condenser heat transfer coefficient on the effective thermal conductivity of the wire sandwiched micro heat pipe are as observed and discussed earlier in the case of triangular micro heat pipes [15, 16].

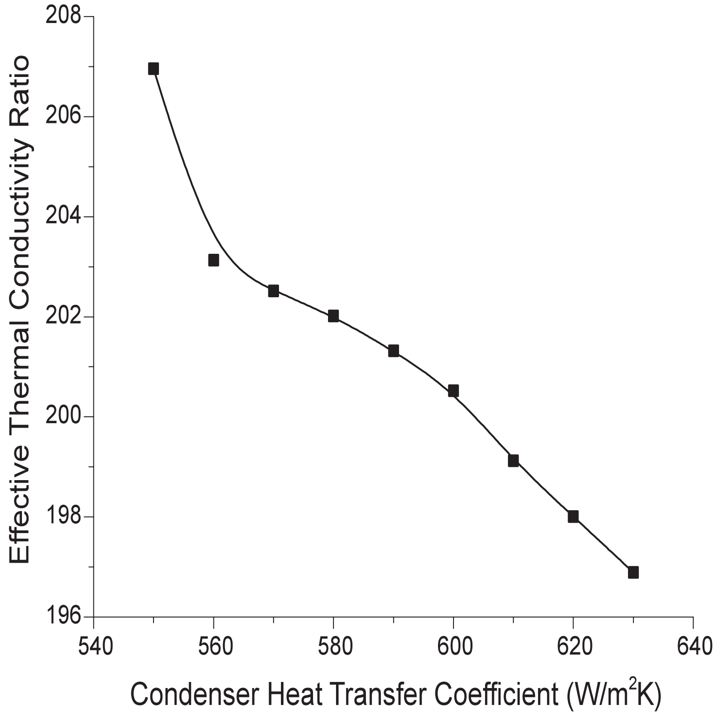

Figure 13. Variation of the effective thermal conductivity ratio (with respect to copper) with the condenser heat transfer coefficient

An increase in either the wire diameter or the pitch of the wires is found to reduce the effective thermal conductivity, due to a larger temperature drop as shown in Figure 14. When the wire diameter or the pitch of the wire is increased, the cross sectional area of the channel is increased. This essentially reduces the flow velocities and the performance. As shown in Figure 15 and Figure 16, the reduction in effective thermal conductivity is more prominent in the case of an increase in the pitch of the wires. This is so, because the liquid cross sectional area is significantly affected due to an increase in the wire diameter, whereas an increase in the pitch does not change the liquid cross section, as the corner shape is unaffected. The variations in the fluid cross sectional areas, upon changing the wire diameter and pitch are given in Table 2, which explains this effect further.

Keeping the total length of the micro heat pipe the same, the lengths of the adiabatic section and the condenser have been simultaneously varied, and calculations performed to obtain the temperature distribution. As shown in Fig 17, it is observed that a decrease in the length of the adiabatic section and an increase in the length of the condenser result in a larger temperature drop between the ends, and a corresponding decrease of the effective thermal conductivity. An increase in the condenser section is found to produce similar effect, as due to an increase in the condenser heat transfer coefficient due to enhanced heat dissipation at the condenser section.

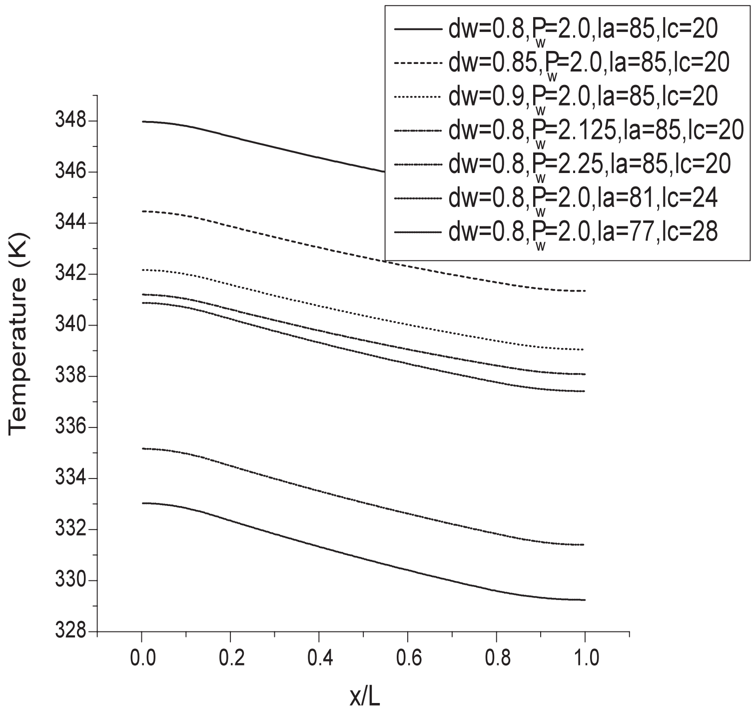

Figure 14. Steady – state temperature distributions for various design parameters

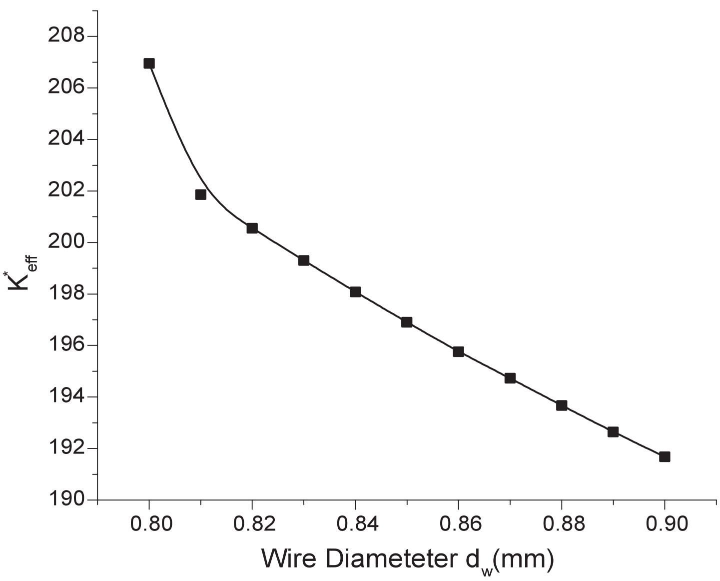

Figure 15. Variation of the effective thermal conductivity ratio with the wire diameter, for an input heat flux of 2.5W/cm^2 and a condenser heat transfer coefficient of 550 W/m^{2}K

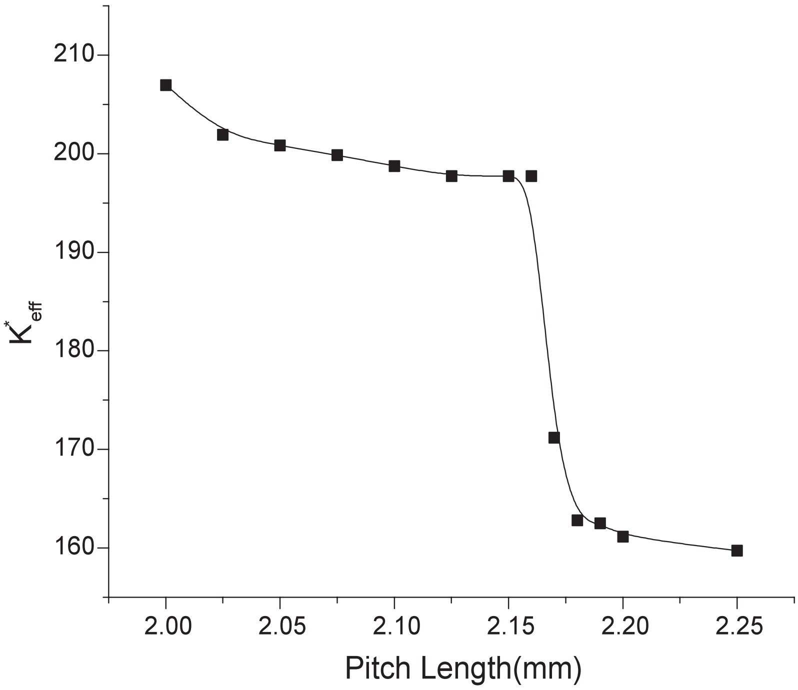

Figure 16. Variation of the effective thermal conductivity ratio with the pitch of the wires, for an input heat flux of 2.5W/cm^2 and a condenser heat transfer coefficient of 550 W/m^{2}K.

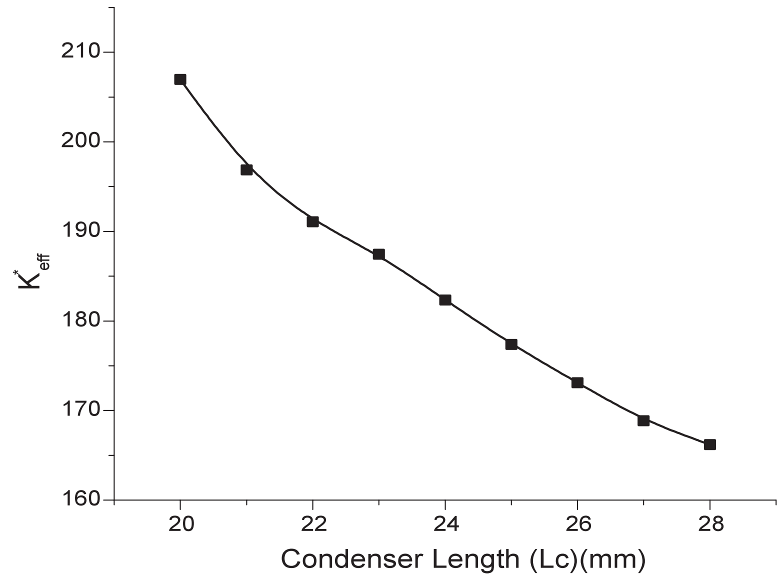

Figure 17. Variation of the effective thermal conductivity ratio with the length of the condenser for a given total length of the micro heat pipe

Table 2 Effect of change in the wire diameter and pitch on the flow areas and the effective thermal conductivity values

Geometric Parameter	Dimension (mm)	Liquid cross-sectional area at the end of the condenser Al (mm^2)	Vapor cross-sectional area at the end of the condenser Av (mm^2)	Total cross-sectional area of the flow passage at the end of the condenser (mm^2)	k_{eff} (W/mK)
Wire diameter	0.8	0.2315	0.8658	1.0973	24570
	0.825	0.2389	0.8765	1.1154	23647
	0.85	0.2462	0.8863	1.1325	22647
	0.875	0.2535	0.8952	1.1487	22361
	0.9	0.2606	0.9032	1.1638	21819
Pitch	2.0	0.2315	0.8658	1.0973	24570
	2.1	0.2315	0.9458	1.1813	24088
	2.2	0.2315	1.0268	1.2583	23889
	2.3	0.2315	1.1058	1.3363	21935

6. OPTIMIZATION STUDY

As discussed in the previous section, various operational and geometric parameters are found to influence the performance of the wire-sandwiched micro heat pipe, as indicated by their effects on the effective thermal conductivity. The numerical results on the parametric studies have been post-processed, first to correlate the performance with the influencing parameters, and then to use this correlation as an objective function to get an optimal combination of the parameters which would give the best performance (in terms of the maximum effective thermal conductivity), within a given range of these parameters.

A multiple linear regression analysis was performed on the numerical results, to establish a between the parameters, which include the evaporator heat flux, the condenser heat transfer coefficient, the pitch and diameter of the wire and the length of the condenser. It was found that the length of the adiabatic section has no significant effect on the effective thermal conductivity, and does not appear in the correlation. The regression was performed using a commercial package (SPSS) which resulted in the following correlation:

$$k_{eff} = 265578.2 + 3.4169\, d_w - 69.472\, h_0 - 68706\, d_w - 67844.4\, P_w - 2163.202 L_c \qquad (28)$$

Within a given range of each of the parameters, the combination which would result in the maximum effective thermal conductivity can be found out by performing an optimization, using the above expression for the effective thermal conductivity as the objective function. For the range of parameters shown in Table 3, this has been performed using the commercial software TORA, which has been recommended in the literature [21]. In this analysis, the value of the evaporator length is kept as a fixed constraint, as in a realistic physical system this represents the length dimension of a heat dissipating surface on which the heat pipe is mounted, which is a fixed quantity. The optimum values of the geometrical and operational parameters and the corresponding value of the effective thermal conductivity obtained within the range of parameters are tabulated in Table 4.

Table 3. Effective thermal conductivity values for different combinations of the operational and the geometrical parameters

q (W/m^2)	h_0 (W/m^{2}K)	d_w (mm)	P_w (mm)	La (mm)	Lc (mm)	k_{eff} (W/mK)
24000.00	550.00	.80	2.000	85.00	20.00	75519.00
24100.00	550.00	.80	2.000	85.00	20.00	75833.00
24200.00	550.00	.80	2.000	85.00	20.00	76148.00
24300.00	550.00	.80	2.000	85.00	20.00	76442.00
24400.00	550.00	.80	2.000	85.00	20.00	76756.00
24500.00	550.00	.80	2.000	85.00	20.00	77071.00
24600.00	550.00	.80	2.000	85.00	20.00	77385.00
24700.00	550.00	.80	2.000	85.00	20.00	77700.00
24800.00	550.00	.80	2.000	85.00	20.00	78014.00
24900.00	550.00	.80	2.000	85.00	20.00	78332.00
25000.00	550.00	.80	2.000	85.00	20.00	78644.00
25000.00	560.00	.80	2.000	85.00	20.00	77189.00
25000.00	570.00	.80	2.000	85.00	20.00	77187.00
25000.00	580.00	.80	2.000	85.00	20.00	77187.00
25000.00	590.00	.80	2.000	85.00	20.00	77187.00
25000.00	600.00	.80	2.000	85.00	20.00	77187.00
25000.00	610.00	.80	2.000	85.00	20.00	77187.00
25000.00	620.00	.80	2.000	85.00	20.00	77142.00
25000.00	630.00	.80	2.000	85.00	20.00	77098.00
25000.00	640.00	.80	2.000	85.00	20.00	63581.00
25000.00	550.00	.81	2.000	85.00	20.00	76708.00
25000.00	550.00	.82	2.000	85.00	20.00	76209.00
25000.00	550.00	.83	2.000	85.00	20.00	75735.00
25000.00	550.00	.84	2.000	85.00	20.00	75270.00
25000.00	550.00	.85	2.000	85.00	20.00	74823.00
25000.00	550.00	.86	2.000	85.00	20.00	74389.00
25000.00	550.00	.87	2.000	85.00	20.00	73999.00
25000.00	550.00	.88	2.000	85.00	20.00	73594.00
25000.00	550.00	.89	2.000	85.00	20.00	73204.00
25000.00	550.00	.90	2.000	85.00	20.00	72840.00
25000.00	550.00	.80	2.025	85.00	20.00	76723.00
25000.00	550.00	.80	2.050	85.00	20.00	76313.00
25000.00	550.00	.80	2.075	85.00	20.00	75939.00
25000.00	550.00	.80	2.100	85.00	20.00	75518.00
25000.00	550.00	.80	2.125	85.00	20.00	75140.00
25000.00	550.00	.80	2.150	85.00	20.00	74778.00
25000.00	550.00	.80	2.175	85.00	20.00	61522.00
25000.00	550.00	.80	2.200	85.00	20.00	61237.00
25000.00	550.00	.80	2.250	85.00	20.00	60700.00
25000.00	550.00	.80	2.000	77.00	28.00	63155.00
25000.00	550.00	.80	2.000	78.00	27.00	64172.00
25000.00	550.00	.80	2.000	79.00	26.00	65783.00
25000.00	550.00	.80	2.000	80.00	25.00	67404.00
25000.00	550.00	.80	2.000	81.00	24.00	69292.00
25000.00	550.00	.80	2.000	82.00	23.00	71232.00
25000.00	550.00	.80	2.000	83.00	22.00	72610.00
25000.00	550.00	.80	2.000	84.00	21.00	74805.00

Table 4 Optimum parameters for maximum effective thermal conductivity

Input Heat Flux	2.5 W/cm^2
Condenser Heat Transfer Coefficient	550 W/m^{2}K
Wire Diameter	0.8 mm
Pitch of the wires	2.0 mm
Length of the Condenser	20 mm
Maximum effective thermal conductivity	78850.96 W/mK

7. CONCLUSIONS

A computational analysis is performed for exploring the fluid flow and heat transfer in a wire sandwiched micro heat pipe, which is a novel design in micro heat pipes. The mathematical model is solved using a fully implicit finite difference scheme and the results are utilized for characterizing the performance through an estimation of the effective thermal conductivity. The major outcomes of the investigation are listed below:

1. It is observed that the meniscus radius of the liquid – vapor interface is minimum at the beginning of the evaporator and maximum at the end of the condenser.
2. An increase in the diameter and pitch of the wires is found to decrease the effective thermal conductivity of the wire-sandwiched micro heat pipe.
3. The velocity, temperature and pressure distributions in the wire-sandwiched design are found to be similar to those in conventional triangular micro heat pipe channels.
4. The effects of various operational and design parameters on the effective thermal conductivity have been correlated and used in optimizing the wire-sandwiched micro heat pipe design for a given range of parameters. The optimization procedure, in general, can be used in the design of the best performing wire-sandwiched micro heat pipes for specific applications, within a prescribed range of operational and geometric parameters.

REFERENCES

1. Garimella, S. V., and Sobhan, C. B., Recent Advances in the Modeling and Applications of Nonconventional Heat Pipes, *Advances in Heat Transfer*, 2001,Vol 35, pp. 249-308.
2. Cotter, T. P., Principles and Prospects of Micro Heat Pipes, *Proceedings of the 5th International. Heat Pipe Conference*, Tsukuba, Japan, 1984, pp. 328-335.
3. Peterson, G. P., and Sobhan, C. B., Applications of Microscale Phase Change Heat Transfer: Micro Heat Pipes and Micro Heat Spreaders, *The MEMS Handbook, 2nd ed., Vol. 3 Applications*, CRC Press Inc., USA, 2005.
4. Babin, B. R., Peterson, G. P., and Wu, D., Steady-state Modeling and Testing of a Micro Heat Pipe, *ASME Journal of Heat Transfer*, 1990, Vol. 112, pp. 595-601.
5. Sobhan, C. B., and Peterson, G. P., *Microscale and Nanoscale Heat Transfer – Fundamentals and Engineering Applications*, Taylor and Francis/CRC Press, 2008.
6. Chi, S. W., *Heat Pipe Theory and Practice*, McGraw-Hill Publishing Company, New York, NY., 1976.
7. Wang, Y. X., and Peterson, G. P., Analysis of Wire – Bonded Micro Heat Pipe Arrays, *AIAA. Journal of Thermophysics and Heat Transfer,* 2002, Vol. 16, No. 3, pp. 346–355.
8. Khrustalev, D., and Faghri, A., Thermal Analysis of a Micro Heat Pipe, *ASME Journal of Heat Transfer*, 1994, Vol. 116, pp. 189-198.
9. Wu, D., and Peterson, G. P., Investigation of the Transient Characteristics of a Micro Heat Pipe, *AIAA Journal of Thermophysics and Heat Transfer*, 1991, Vol. 5, pp. 129-134.
10. Wu, D., Peterson, G. P., and Chang, W. S., Transient Experimental Investigation of Micro Heat Pipes, *AIAA Journal of Thermophysics and Heat Transfer*, 1991, Vol. 5, pp. 539-545.

11. Longtin, J. P., Badran, B., and Gerner, F.M., A One-Dimensional Model of a Micro Heat Pipe During Steady-State Operation, *ASME Journal of Heat Transfer*, 1994, Vol. 116, pp. 709-715.
12. Peterson, G. P., and Ma, H. B., Temperature Response and Heat Transfer in a Micro Heat Pipe, *ASME Journal of Heat Transfer*, 1999, Vol. 121, pp. 438-445.
13. Hopkins, R., Faghri, A., and Khrustalev, D., Flat Miniature Heat Pipes with Micro Capillary Grooves, *ASME Journal of Heat Transfer*, 1999, Vol. 121, pp. 102-109.
14. Ma, H. B., Peterson, G. P., and Peng, X. F., Experimental Investigation of Counter-current Liquid-Vapor Interactions and its Effect on the Friction Factor, *Experimental Thermal and Fluid Science*, 1996, Vol. 12, pp. 25-32.
15. Sobhan, C. B., Xiaoyang, H., and Yu, L. C., Investigations on Transient and Steady State performance of micro heat pipe, *AIAA Journal of. Thermophysics and Heat transfer*, 2000, Vol. 14, pp. 161-169
16. Sobhan, C. B., and Peterson, G. P., Modeling of the Flow and Heat Transfer in Micro Heat Pipes, *Second International conference on Microchannels and Minichannels*, Rochester, NY, 2004.
17. Sobhan, C. B., Rag, R. L., and Peterson, G. P., A Review and Comparative Study of the Investigations on Micro Heat Pipes, *International Journal of Energy Research*, 2007, Vol. 31, pp. 664–688.
18. Launay, S., Sartre, V., and Lallemand, M., Investigation of a Wire Plate Micro Heat Pipe Array, *International Journal of Thermal Sciences*, 2004,Vol. 43, pp. 499-507.
19. Bejan, A., *Convection Heat Transfer*, 3rd ed., John Wiley & Sons, Inc, Hoboken, New Jersey, 2004.
20. Vadakkan, U., Garimella, S.V., and Sobhan, C. B., *Characterization of Performance of Flat Heat Pipes for Electronics Cooling*, EEP Vol.28, Packaging of Electronic and Photonic Devices, ASME, 2000.
21. Taha, H., *Operations Research: An Introduction*, 7th edn., Prentice Hall, Inc., Upper Saddle River, New Jersey, 2003.